Fracture Simulations in C-SAFE

Fracture Simulations in C-SAFE

John A. Nairn* and Honglai Tan
Material Science & Engineering, University of Utah, Salt Lake City, UT 84112, U.S.A

January 11, 2001

INTRODUCTION

By necessity, the Center for Simulations of Accidental Fires and Explosions (C-SAFE) must model fracture during explosion events. First, it is self-evident that before something explodes it must break into pieces which involves many fracture events and large amounts of crack propagation. Second, the C-SAFE accident scenarios involve combustion reactions. Because combustion occurs preferentially on free surfaces and fracture creates new free surfaces, physically correct simulations of combustion should track explicit cracks and couple the formation of new cracks to the enhancement of more combustion. Despite these comments, explicit modeling of cracks and crack propagation in large-scale simulations can be a numerically *expensive* task. A common practice is to admit that fracture is too complicated and replace explicit crack modeling with empirical, continuum approaches such as *effective* damage parameters. One goal of C-SAFE is to make use of massively-parallel, advanced super computers to be able to more realistically model cracks and fracture processes in large-scale simulations.

This document highlights some results from the fracture group in C-SAFE. Most of the effort to date, has be placed on modifying the material point method (MPM) to give accurate results for fracture calculations and to be able to handle explicit, internal cracks. MPM has only recently be adapted for solid mechanics problems; it had not previously be used for fracture modeling. In C-SAFE, we have developed adaptive mesh algorithms, node visibility methods, and broken cell shape functions, that together can explicitly model crack propagation in MPM simulations. Because the C-SAFE problems involve temperature gradients, we have also coupled mechanics and thermal conductivity calculations to be sure we include all mechanical and thermal effects in the crack propagation process.

The selection of MPM by C-SAFE was a *group* decision that was based on the overall needs of the center simulations. MPM was *not* selected with fracture calculations in mind; in fact, MPM has initially been a hindrance to inclusion of explicit cracks. A by product of our modification of MPM for fracture, however, is that MPM many turn out to be a powerful new tool in dynamic fracture mechanics problems. As explained briefly below, our modified MPM can simultaneously handle opened and closed explicit cracks. By using adaptive mesh methods, a single simulation can track large amounts of crack propagation. Finally, the crack path is free to follow its natural direction instead of being limited to predefined mesh directions.

FRACTURE IN MPM

The material point method (MPM) is an extension of techniques first used in fluid mechanics[1–4] to now solve problems in solid mechanics.[9–11] As shown in Fig. 1A, MPM discretizes the specimen into a collection of material points instead of into elements as done in finite element analysis (FEA). Each material point is given a mass, assigned an initial "state" (*e.g.*, stress, strain, strain rate, position, velocity, temperature, *etc.*) and assigned material-response properties. The thermal and mechanical material response is determined by constitutive laws that can take any form. An MPM analysis involves simultaneously integrating the equations of motion and heat transfer for the discretized material points. Although MPM already has many capabilities, there were three problems that needed to be solved before it could be used for explicit fracture calculations. First, fracture calculations might require more mesh refinement than previously used in MPM calculations; second, the standard MPM algorithm has some energy dissipation that might affect energy-based fracture calculations; and third, current MPM does not correctly represent internal crack surfaces. The first two problems are discussed in this section; the internal crack representation problem is discussed in the next section.

*Phone:+1-801-581-3413, FAX:+1-801-581-4816, Email:John.Nairn@m.cc.utah.edu

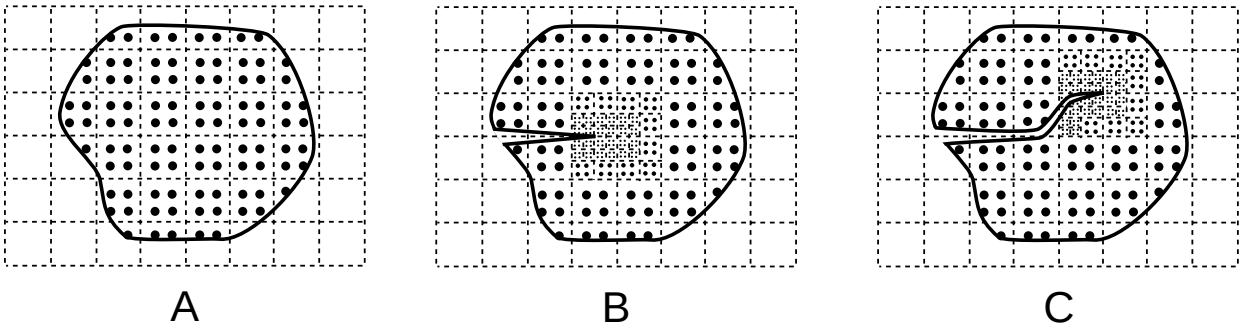

Fig. 1. **A**. A non-adaptive, 2D MPM grid. The dark line is the outline of the specimen and it is discretized into equally spaced and sized material points. The dotted lines are the background calculational grid. **B**. MPM model for crack calculations requiring refinement of the material points around the crack tip. This schematic view shows just three levels of refinement. **C**. As the crack propagates, the adaptive mesh algorithm can merge material points behind the crack tip and create new material points in the new crack tip region.

Previous MPM calculations in solid mechanics have always discretized the material into a regular grid (see Fig. 1A). Such a mesh will certainly be very inefficient for solving large problems that must be able capture all the detail required to handle crack-tip stress states. To solve this problem, we have developed hierarchical tree-structured MPM cell methods for solid mechanics calculations.[5] During the simulation, these new MPM cells can adapt automatically to different local resolution requirements as judged by tracking gradients in local velocity or heat flux. When required, the cells and material points are automatically split. The refinement can continue to finer and finer scales as required by the problem being solved. Because smaller MPM cells require smaller time steps for accurate calculations, our hierarchical, tree-structured, MPM code implements sub-cycling in which the smaller cells update with a smaller time step than the larger cells. A schematic view of a refined mesh around a crack tip is shown in Fig. 1B. MPM adaptivity is especially useful for crack propagation problems. Figure 1C shows the same crack from Fig. 1B after some crack propagation. The adaptivity allows material points to continually refine in new crack tip regions. After the crack passes, the previously refined material points will merge when refinement is no longer needed.

Previous MPM calculations are known to have some energy dissipation. In each MPM time step, the grid accelerations are related to the grid forces through a mass matrix. To avoid inverting the full mass matrix, most MPM simulations use a lumped mass matrix in which the masses in each row are summed and placed on the diagonal. This approach gives excellent results for many problems but may cause a small amount of kinetic energy dissipation.[6] Because fracture calculations rely on energy calculations, it is important to verify that energy dissipation is not a problem or that it can be reduced by new methods. A simple solution is to unlump the mass matrix. Unlumping the entire mass matrix, however, is probably too inefficient and may be unnecessary. An alternative approach is to unlump the mass matrix near crack tips but use a lumped mass matrix in regions that do not require detailed energy calculations.

To demonstrate our hierarchical MPM cells with explicit cracks and to investigate lumped *vs.* unlumped mass matrix calculations, we did some isothermal 2D calculations for a DCB specimen.[5] The specimen geometry and a typical automatically refined mesh are shown in Fig. 2A. At time zero, a load was applied to the ends of the specimen and a full, dynamic MPM calculation was run. At each time step we used crack-closure methods[7] to calculate the dynamic energy release rate ($G(t)$) for crack growth. We did a full dynamic analysis, but included damping in the material response to let $G(t)$ converge to the static G for a DCB specimen. This static result can be calculated by a beam-on-an-elastic-foundation model,[8] which is known, by comparison to numerical calculations, to be essentially an exact result. Figure 2B plots the MPM results for $G(t)$ calculated with a regular grid or a hierarchical grid and calculated with a lumped mass matrix or a full mass matrix. The curve labeled "Unmodified MPM" gives the results for a regular grid and a "lumped" mass matrix; *i.e.*, the result of MPM methods currently documented in the literature.[9–11] This result shows that standard MPM has lower accuracy for fracture calculations. The static $G(t)$ in this analysis differs from the exact result by 24%. Using either a full mass matrix (but still with a regular grid —

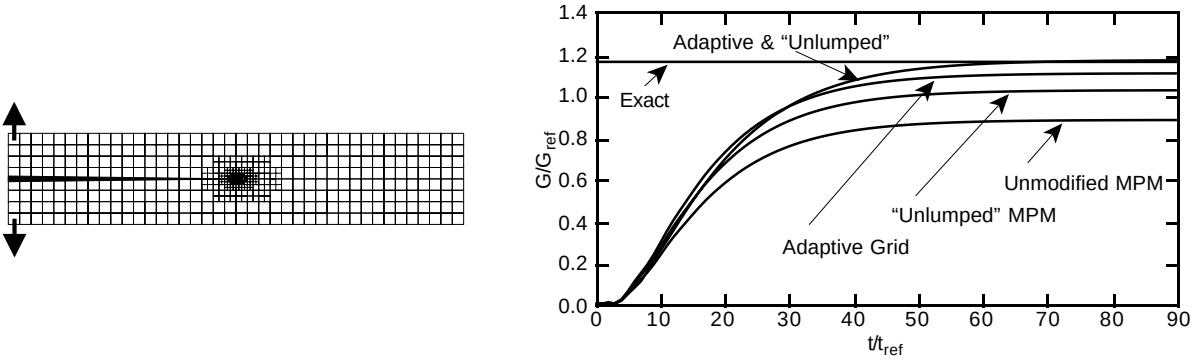

Fig. 2. MPM calculations for energy release rate due to crack growth in DCB specimens. The left side shows the refined MPM mesh (without the four material points per cell). The right side plots dynamic energy release rate calculated by four different methods. The "Adaptive" grid calculations used the mesh refinement shown on the left; the other calculations used the regular grid remote from the crack tip over the entire specimen. All results are normalized to reference conditions based on simple beam theory.

see curve labeled '"Unlumped" MPM') or our hierarchical elements (but still with a lumped mass matrix — see curved label "Adaptive Grid") improves the calculations. Mesh refinement is more effective in improving accuracy then is the full mass matrix. Mesh refinement reduces the error to 5%, while a full mass matrix only reduces the error to 14%. Finally, the combination of hierarchical cells and a full mass matrix (see curve labeled 'Adaptive & "Unlumped"') leads to extremely accurate calculations (within 1% of the exact result).

These results show that our new MPM code is capable of accurate fracture calculations by using hierarchical elements. The best results in Fig. 2B used an inefficient full mass matrix. The fact that mesh refinement was more effective than unlumping the mass matrix gives us confidence that a partially unlumped mass matrix will give efficient and accurate results.

CRACK SURFACES

Finite element analysis and MPM have complementary properties when it comes to dealing with internal crack surfaces. In finite element analysis, one can incorporate cracks in a mesh by breaking connections between elements. Such cracks will automatically be non-interacting surfaces that correctly model opened cracks. They will not work as well, however, if the crack surfaces contact each other. Without nonlinear modifications to the finite element meshes, there is nothing to prevent the crack surfaces from interpenetrating with each other. MPM has the opposite problem. In conventional MPM, particles *see* each other whenever they appear in the same element or in adjacent elements of the background, calculational grid. In other words, MPM automatically prevents crack surfaces from interpenetrating. Because there is nothing in conventional MPM to determine whether or not two particles are actually connected by bulk material, however, particles on opposite sides of opened cracks will think they should interact. In other words, conventional MPM does not correctly model opened cracks. We have modified MPM to handle internal cracks by introducing *node visibility* and *broken cell shape function* concepts. These new methods, which can be incorporated into MPM code with little modifications, extends MPM to model opened cracks. By adding a comparison between the current deformation state and the undeformed state, our new approach can continue to handle crack surface contact. In other words, our modified MPM simultaneously models opened and closed cracks.

Our goal was to develop a method to include explicit cracks in MPM without requiring too much modification of the basic MPM algorithm. To handle internal cracks, each particle is assigned a new property which is a vector normal to the nearby crack surface. Whenever a crack is created and passes by a crack, the normal vector of that particle is set equal to the normal vector of the new crack surfaces. If a particle is not near a surface, the normal vector will be zero. To account for explicit cracks, we use particle-node visibility information to modify the normal shape functions used for field interpolations. Figure 3 shows an example for particle p in an 8-noded, 3D element. From the crack surface plane (which is determined by the

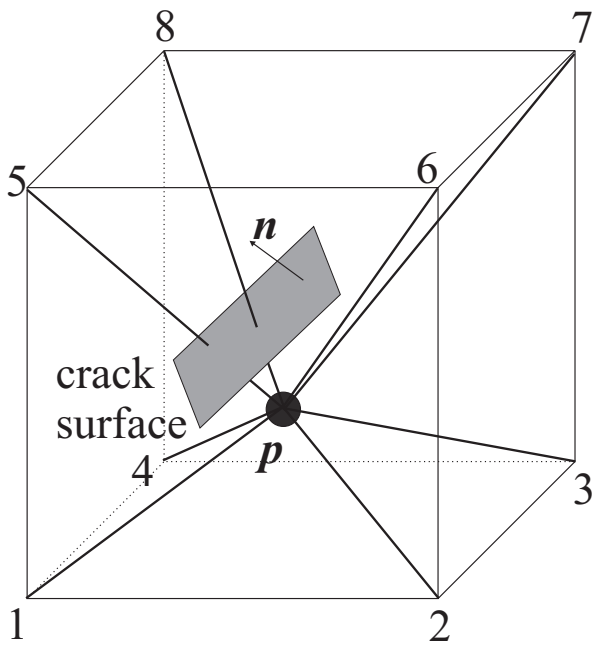

Fig. 3. Crack surface normal.

crack surface normal, $\hat{n}$), we can determine a visibility index for node n as viewed from particle p as

$$Vis^{(n,p)} = \begin{cases} 1 & \text{node } n \text{ on same side of crack as particle } p \\ 0 & \text{node } n \text{ on opposite side of crack as particle } p \end{cases} \tag{1}$$

The total number of visible nodes at particle p can be written as

$$S_{vis}^{(p)} = \sum_{m \in \text{nodes around } p} Vis^{(m,p)} \tag{2}$$

Using these two results, we define modified shape function ($\tilde{N}^{(n,p)}$) which we label as *Broken Cell Shape Functions*. The new shape functions are calculated from the ordinary shape functions ($N^{(n,p)}$) by

$$\tilde{N}^{(n,p)} = Vis^{(n,p)} \left[N^{(n,p)} + \frac{\displaystyle\sum_{m \in \text{nodes around } p} N^{(m,p)} \left(1 - Vis^{(m,p)}\right)}{S_{vis}^{(p)}} \right] \tag{3}$$

These shape function are equal to 1 at each visible node, still sum to 1 throughout the element, and, most importantly, automatically ignore information at invisible nodes (because the associated shape functions are zero) when used in typical MPM code. To simultaneously handle opened and closed cracks, the visibility modifications are turned on or off depending on whether the current particle-particle separations (*i.e.*, unmodified strain interpolations) are closer or farther apart then in the initial material.

THERMAL EFFECTS IN DYNAMIC FRACTURE

As a crack propagates through a material, initially at constant temperature, it will generate heat. Experimental estimates suggest that 60 to 90% of the energy released during fracture gets converted to heat in the crack tip regions.[12, 13] At high enough crack velocity in dynamic fracture problems, there will be insufficient time for the heat to be conducted away from the crack tip. The heating will thus lead to a gradient of

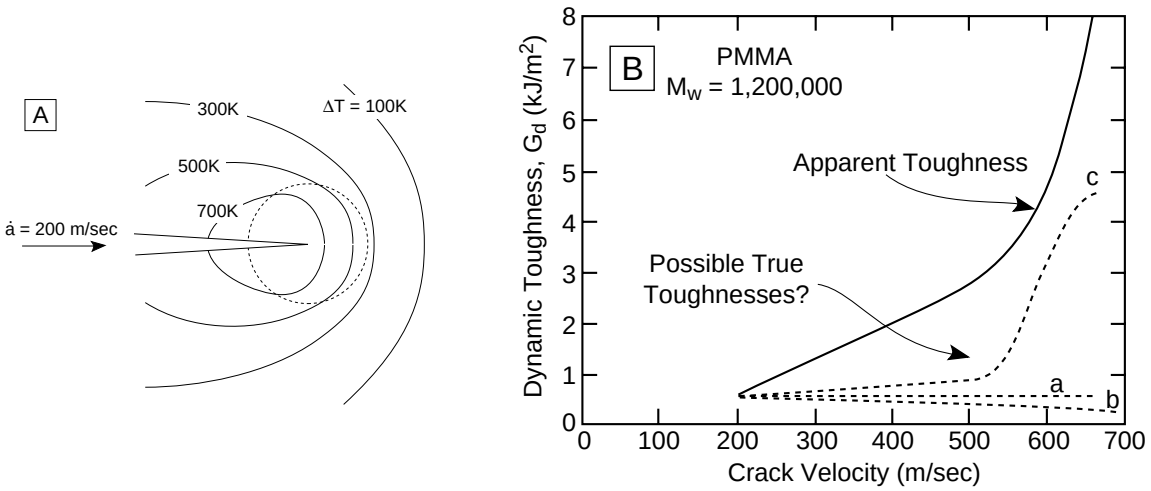

Fig. 4. **A**. Calculated crack tip heating due to crack propagation in glass at 200 m/sec. The circular zone indicates an assumed plastic zone of radius 30Å. The cracking process was assumed to release 2 mJ/m^2. **B**. The dynamic fracture toughness of PMMA. The "Apparent Toughness" was "measured" using a method that ignores thermal effects. Curves a, b, and c are three possible results for the "true toughness" once all thermal effects are included in the analysis of the experiments.

temperature which is locally hot around the crack tip and cooler away from the crack tip. The intensity of the gradient will increase as the crack speed increases or as the thermal conductivity of the material decreases. A thermal gradient influences fracture in two ways. First, the high temperatures can cause the physical properties, including fracture properties, of the material to change. Second, a thermal gradient will induce residual stresses. Because these residual stresses contribute to total energy release rate, they need to be included in a full analysis of dynamic fracture. In other words, dynamic simulations of crack growth must be coupled mechanical and thermal conductivity simulations.

The existence of crack tip heating has long been recognized.[12–21] There are active research efforts aimed at developing experimental methods for observing thermal gradients in dynamic fracture.[21] A good picture and reasonable estimates of crack tip heating can be derived by thermal conduction calculations.[14, 16, 19, 21] The thermal energy balance equation in coupled thermoplasticity is[22]

$$\nabla \cdot k\nabla T - T_0(\boldsymbol{C}\boldsymbol{\alpha}) \cdot \dot{\boldsymbol{\varepsilon}} + \dot{Q} = \rho c \frac{\partial T}{\partial t} \tag{4}$$

where T is temperature, T_0 is the reference temperature, k, $\boldsymbol{C}$, $\boldsymbol{\alpha}$ ρ, and c are the thermal conductivity, stiffness tensor, thermal expansion tensor, density, and heat capacity of the material, $\dot{\boldsymbol{\varepsilon}}$ is the strain rate tensor, and $\dot{Q}$ is the rate of heat production due to plasticity. The second term is a thermoelastic term. For isotropic materials, this term leads to cooling as the material dilates. Some recent experiments in fracture show that this effect can lead to cooling ahead of the crack tip prior to initiation of mode I dynamic fracture.[20] Once the crack begins to propagate, however, heating caused by plastic dissipation at the crack tip and represented by the term $\dot{Q}$ dominates and the temperature of the crack tip region always increases.[20] Equation (4) can be solved analytically for a point (or line) heat source moving at constant velocity in an infinite isotropic material with temperature independent properties and negligible dilational cooling.[23] The point-source solution has a singular temperature at the crack tip. The singularity can be resolved by spreading the heat dissipation over a finite-sized plastic zone.[14, 16] Weichert and Schönert, used this approach to calculate crack tip heating in glass;[14] a typical steady-state temperature field is shown in Fig. 4A. The crack tip temperature rise of over 700K is very large and the thermal gradients are steep.

Despite the well-known high temperatures possible at crack tips, the detailed inclusion of thermal effects in dynamic fracture analysis remains relatively unexplored. There are two ways thermal effects are commonly ignored. First, in dynamic fracture mechanics experiments, the critical stress intensity factor is often determined from experimental results for failure load and crack velocity by using elastodynamic stress analysis of

a propagating crack.[24, 25] The commonly-used elastodynamic analyses are isothermal analyses that do not account for thermal gradients at the crack tip. Any fracture toughness determined by this approach will thus be an *apparent* toughness. Second, there are powerful optical techniques such as Moire interferometry, the method of caustics, and coherent gradient sensor methods for dynamic fracture experiments.[26–28] Although these powerful techniques are sometimes mislabeled as "measuring" dynamic stress intensity factors, they work be detecting gradients in the out-of-plane displacements. The experimental results for displacement get *converted* to stress intensity factor by making use of an asymptotic expansion for the relation between crack tip stresses and out-of-plane displacements. When this relation ignores crack-tip thermal gradients, as it always does, the so-called measured fracture parameters again represent apparent results. The residual stresses caused by crack-tip thermal gradients, however, will contribute to the singular stresses and thus must be included before optical methods can give *true* fracture parameters for propagating cracks.

What is the consequence of ignoring thermal effects? Figure 4B shows some early results for the dynamic fracture toughness of PMMA.[12] As is commonly reported for polymers, the dynamic toughness is an *increasing* function of crack velocity. This dependence on crack velocity in contrary to common experience with polymer failure in which most polymers become more brittle, hence lower in toughness, at higher rates. It is important to recognize that the literature results in Fig. 4B, however, are an apparent toughness because they were deduced from an isothermal analysis of crack growth.[29] If one could measure *true* toughness, the results might change and our understanding of dynamic polymer fracture might change too.

The question remains — what happens to the *true* toughness as a function of crack speed? Figure 4B suggest three possible scenarios for dynamic polymer fracture toughness. Curve *a* corresponds to a material for which the true toughness is independent of crack speed. Such a result implies that the entire difference between apparent and true toughness is due to crack-tip residual stresses induced by crack tip heating. Because crack tip heating leads to compressive residual stresses, it should always inhibit fracture and cause the apparent toughness to be too high. The error in apparent toughness will get larger as the crack speed increases. It is thus certain that the true dynamic toughness will increase less with crack speed than currently reported apparent results.

Perhaps, like curve *a*, the true toughness is independent of crack velocity — but it may be otherwise. Curve *b*, for example, shows a true toughness that decreases with crack speed; this toughness agrees better with other rate-dependent effects in deformation of PMMA (the material for Fig. 4). Finally, Curve *c* shows a hypothetical result for a material that undergoes a thermal transition at a crack speed of about 550 m/sec. Such a result might be caused by temperature-dependent material properties. Notice that the reported apparent toughness also starts increasing more rapidly at 550 m/sec. This rapid increase might be due to a thermal transition in PMMA (such as its glass transition). The transition, however, is masked by the analysis method that produces only apparent toughness results.

To consider general dynamic fracture with complete inclusion of thermal effects, we have written our, 3D, parallel MPM code with hierarchical elements, partially unlumped mass matrices, and explicit cracks to do coupled mechanical and thermal conductivity calculations. This code can be used to simulate a wide variety of crack growth problems and to assess the importance of thermal effects in interpretation of the dynamic fracture experiments. Contrary to the common approach in dynamic fracture of assuming a constant crack velocity, our simulations can propagate the crack according to an energy release rate criterion. In other words, the crack will propagate when the current dynamic energy release rate exceeds the *true* toughness for the material. In simulations, the true toughness can either be independent of crack velocity and temperature or it can be allowed to have arbitrary dependence on crack velocity and temperature. Whenever the crack propagates, it will release some fraction (a parameter, but probably close to 100% for most materials) of the actual energy released to heat in the crack-tip region. Finally, all material properties can be temperature dependent properties in order to simulate to role of physical changes caused by crack-tip heating.

The plot in Fig. 5 is sample output from our MPM code. This calculation is for a crack running in polymer that follows a Mooney-Rivlin constitutive low. This crack was assumed to propagate when the dynamic $G(t)$ was equal to the toughness of the material which was taken as $G_c = 100$ J/m^2. In this preliminary result, G_c was assumed to be independent of crack velocity and 100% of the released energy was converted to heat. The specimen was a double cantilever beam and the input loading conditions caused a nearly constant crack velocity of 100 m/sec. The maximum crack tip temperature rise was $\Delta T = 1100$K. This result is artificial because all material properties were taken as independent of temperature and no polymer can withstand 1100K temperature rise. The result confirms, however, that large temperature rises will occur in dynamic

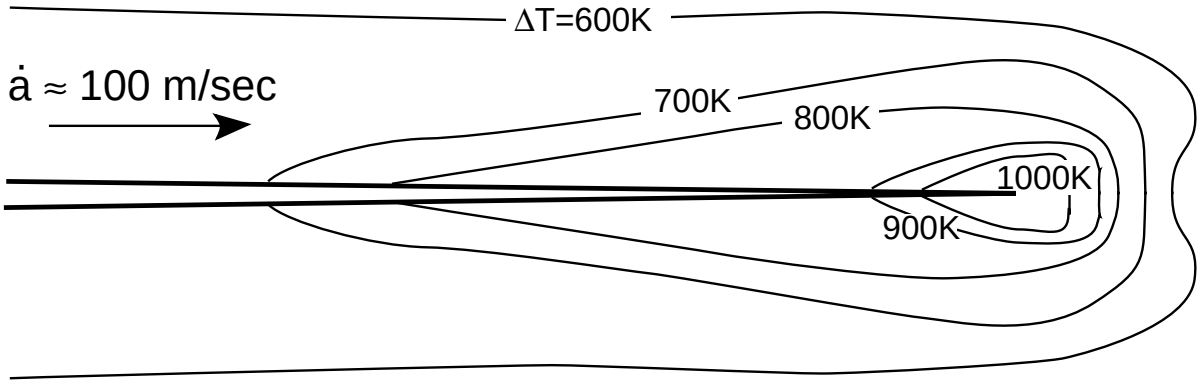

Fig. 5. The transient temperature field around a crack growing at about 100 m/sec in a typical polymer following a Mooney-Rivlin constitutive law in which all the fracture energy ($G_c = 100$ J/m^2) is released as heat.

fracture and demonstrates our code that does coupled mechanical and thermal calculations for fracture.

C-SAFE FRACTURE OR COMBUSTION-ASSISTED CRACK GROWTH

Fracture simulations in C-SAFE involve crack growth in the presence of crack surface combustion reactions. This type of crack growth has not be well studied. The methods described in the previous three sections, however, provide all the tools needed for inclusion of combustion effects. First, our modified MPM methods can now include explicit cracks and do fracture calculations. This step is important because combustion occurs preferentially on crack surface. When combustion does occur it will produce both thermal and mechanical energy. The thermal energy will provide heat to crack surfaces. Our techniques of coupling mechanical and thermal conductivity will accept the combustion heat energy as input to the thermal part of the problem. Combustion by-products in the form of gases will provide mechanical energy by pressurizing the crack surfaces. Our method to include explicit cracks can include this pressure by adding boundary conditions to the particles near crack surfaces. Because gas pressure will cause cracks to open, it is important that we have modified MPM using *node visibility* and *broken cell shape functions* to correctly model opened cracks. Finally, combustion-assisted cracks are a new type of dynamic fracture problem. Combustion occurs on crack surfaces and crack propagation produces more crack surface. Thus, crack growth will lead to more combustion which will promote more crack growth. The resulting positive feedback is expected to lead to new phenomena such as crack growth faster than the Rayleigh wave speed in the material.

REFERENCES

1. Brackbill, J. U., and H. M. Ruppel, FLIP: A Method for Adaptively Zoned, Particle–in–Cell Calculations of Fluid Flows in Two Dimensions. *J. Comp. Phys.*, 1986, **65**, 314–343.
2. Brackbill, J. U., D. B. Kothe, and H. M. Ruppel, FLIP: A Low Dissipation, Particle–in–Cell Method for Fluid Flow. *Comp. Phys. Comm.*, 1988, **48**, 25–38.
3. Brackbill, J. U., and G. Lapenta, A Method to Suppress the Finite–Grid Instability in Plasma Simulations. *J. Comp. Phys.*, 1994, **114**, 77–84.
4. Lapenta, G., and J. U. Brackbill, Control of the Number of Particles in Fluid and MHD Particle in Cell Methods. *Comp. Phys. Comm.*, 1995, **87**, 139–154.
5. Tan, H. and J. A. Nairn, Hierarchical Adaptive Material Point Method in Dynamic Energy Release Rate Calculations. *Comput. Meths. Appl. Mech. Engrg.*, 2000, **in preparation**.
6. Burgess, D., D. L. Sulsky, and J. U. Brackbill, Mass matrix formulation of the FLIP particle–in–cell method. *J. Comp. Phys.*, 1992, **103**, 1–15.

7. Rybicki, E. F. and M. F. Kanninen, A Finite Element Calculation of Stress Intensity Factors By a Modified Crack Closure Integral. *Eng. Fract. Mech.*, 1977, **9**, 931–938.
8. Kanninen, M. F., An Augmented Double Cantilever Beam Model for Studying Crack Propagation and Arrest. *Int. J. Fract.*, 1973, **9**, 83–92.
9. Sulsky, D., Z. Chen, and H. L. Schreyer, A Particle Method for History-Dependent Materials. *Comput. Methods Appl. Mech. Engrg.*, 1994, **118**, 179–196.
10. Sulsky, D., S.-J. Zhou, and H. L. Schreyer, Application of a Particle-in-Cell Method to Solid Mechanics. *Comput. Phys. Commun.*, 1995, **87**, 236–252.
11. Sulsky, D., and H. L. Schreyer, Axisymmetric Form of the Material Point Method with Applications to Upsetting and Taylor Impact Problems. *Comput. Meths. Appl. Mech. Engrg.*, 1996,, **139**, 409–429.
12. Döll, W., Application of an Energy Balance and an Energy Method to Dynamic Crack Propagation. *int. J. Fract.*, 1976, **12**, 595–605.
13. Y. K. Gudovsky, *Thermophysical Properties of Polymers*, Springer-Verlag, Berlin (1992).
14. Weichert, R. and K. Schonert, On the Temperature rise at the Tip of a Fast Running Crack. *J. Mech. Phys. Solids*, 1974, **22**, 127–133.
15. Fuller, K. N. G., P. G. Fox, and J. E. Field, The Temperature Rise at the Tip of a Fast-Moving Crack in Glassy Polymers. *Proc. Roy. Soc. London*, 1975, **A341**, 537–557.
16. Weichert, R. and K. Schonert, Heat Generation at the Tip of a Moving Crack. *J. Mech. Phys. Solids*, 1978, **26**, 151–161.
17. Williams, J. G. and J. M. Hodgkinson, Crack-Blunting Mechanisms in Impact Tests on Polymers. *Proc. R. Soc. London A*, 1981, **375**, 231–248.
18. Zehnder, A. T. and A. J. Rosakis, On the Temperature Distribution at the Vicinity of Dynamically Propagating Cracks in 4340 Steel. *J. Mech. Phys. Solids*, 1991, **39**, 385–415.
19. Mason, J. J. and A. J. Rosakis, On the Dependence of the Dynamic Crack Tip Temperature Fields in Metals Upon Crack Tip Velocity and Material Parameters. *Mechanics of Materials*, 1993, **16**, 337–350.
20. Rittel, D., Thermomechanical Aspects of Dynamic Crack Initiation. *Int. J. Fract.*, 1999, **99**, 199–209.
21. Zehnder, A. T., K. S. Bawa-Bhallay, R. Thomas, and L. D. Favroz, Thermal Analysis of Crack Tearing. *International Congress of Theoretical and Applied Mechanics*, August 27 - September 2, 2000, Chicago, 2000.
22. Carlson, D. E., Linear Thermoelasticity. *Mechanics of Solids, Volume II*, ed., C. Truesdell (ed.), Springer-Verlag, New York, 1984, 297–345.
23. Rosenthal, D., The Theory of Moving Sources of Hear and its Application to Metal Treatments. *Trans ASME*, 1946, **68**, 849–866.
24. Freund, L. B., *Dynamic Fracture Mechanics,* Cambridge University Press, New York (1990).
25. Kanninen, M. F., and C. H. Popelar, *Advanced Fracture Mechanics,* Oxford University Press, New York (1985).
26. Kalthoff, J. F., W. Boehmem, and S. Winkler, Analysis of Impact Fracture Phenomena by Means of the Shadow Optical Method of Caustics. *Proc. 7th Int. Conf. on Experimental Stress Analysis*, Haifa, Israel, 1982.
27. Tippur, H. V., S. Krisnaswamy, and A. J. Rosakis, A Coherent Gradient Sensor for Crack-Tip Deformation Measurements: Analysis and Experimental Results. *Int. J. of Fract.*, 1991, **48**, 193–204.
28. Tippur, H. V. and S. Ramaswamy, Measurement of Mixed-Mode fracture Parameters Near Cracks in Homogeneous and Bimaterial Beams. *Int. J. Fract.*, 1993, **61**, 247–265.
29. Broberg, K. B., The Propagation of a Brittle Crack. *Arkiv for Physik*, 1960, **18**, 159–192.